IEEE Access
Multidisciplinary | Rapid Review | Open Access Journal

Received January 29, 2021, accepted February 17, 2021, date of publication February 23, 2021, date of current version March 4, 2021.

Digital Object Identifier 10.1109/ACCESS.2021.3061429

Enabling NOMA in Backscatter Reconfigurable Intelligent Surfaces-Aided Systems

CHI-BAO LE[1], DINH-THUAN DO[2], (Senior Member, IEEE), XINGWANG LI[3], (Senior Member, IEEE), YUNG-FA HUANG[4], (Member, IEEE), HSING-CHUNG CHEN[2,5], (Senior Member, IEEE), AND MIROSLAV VOZNAK[6], (Senior Member, IEEE)

[1]Faculty of Electronics Technology, Industrial University of Ho Chi Minh City (IUH), Ho Chi Minh City 700000, Vietnam
[2]Department of Computer Science and Information Engineering, Asia University, Taichung 41354, Taiwan
[3]School of Physical and Electronics Engineering, Henan Polytechnic University, Jiaozuo 454003, China
[4]Department of Information and Communication Engineering, Chaoyang University of Technology, Taichung 413310, Taiwan
[5]Department of Medical Research, China Medical University Hospital, China Medical University, Taichung 40402, Taiwan
[6]Department of Telecommunications, VSB-Technical University of Ostrava, 70833 Ostrava, Czech Republic

Corresponding author: Dinh-Thuan Do (dodinhthuan@asia.edu.tw)

This work was supported by the Ministry of Education, Youth and Sport of the Czech Republic within the grant SP2020/65 conducted at the VSB-Technical University of Ostrava. The work of Dinh-Thuan Do was supported by the Ministry of Science and Technology (MOST), Taiwan, under Grant MOST 110-2222-E-468-001.

ABSTRACT One of the key enablers of future wireless communications is constituted by massive users can access the core network in wireless systems simultaneously, which can improve the spectral efficiency. In existing scheme of massive connections, namely non-orthogonal multiple access (NOMA), is investigated in conventional relaying networks. This method results in excessive power consumption and high hardware costs. Recently, reconfigurable intelligent surface (RIS) has been considered as one of the revolutionary technologies to enable energy-efficient and smart wireless communications, which is a two-dimensional structure with a large number of passive elements. This paper examines the RISs used in emerging communications systems based on NOMA scheme. The two-user system model contains the far user and the near user which employing RIS and NOMA is conducted in this study. In particular, we design two links (backscatter and direct links) to target to improve performance of far user. System performance was characterized through closed-form expressions of outage probability, ergodic capacity and throughput, which are beneficial to evaluate performance of two users. In Monte-Carlo simulations, it was revealed that the probability of the two users experiencing system outage was determined by factors related to power allocation, power transmission at the base station, and the number of reflecting elements in the RISs.

INDEX TERMS Reconfigurable intelligent surface (RIS), NOMA, outage probability, ergodic capacity.

I. INTRODUCTION

The commercialization of fifth generation (5G) wireless communication systems faces the crucial challenges in terms of high energy consumption and reduced network deployment cost. Recently, considering as low manufacturing, hardware and energy cost the reconfigurable intelligent surface (RIS) leads to special attentions from researchers [1-3]. As a promising approach to overcome the existing challenges, the RISs are able to adjust the phase shift of the incident signal by enabling a planar array containing a large number of low-cost reconfigurable reflecting elements. Therefore, the RIS can generate a directional beam by reflecting the incident signal and thus improving the coverage and link quality and. In addition, the RIS can benefit from reflecting signal and the direct signal targeting to the intended user to substantially enhance the strength of received signal. If amplify-and-forward (AF) relaying and backscatter communications are studied in the literature, then they are significant difference with RIS due to new techniques developed. For instance, the RIS only passively reflects the incident signal without generating its own transmission signal, which is different with AF relaying, and thus enhancing power consumption. In contrast with the backscatter communications, the RIS does not send its own information. In particular, RIS only operates as a helper to improve the performance

The associate editor coordinating the review of this manuscript and approving it for publication was Anton Kos.

of existing links [2], [4]–[6]. Generally, the advantages of energy-efficient and cost-effective in the RIS is reported by abundant reconfigurable reflecting elements. By inducing a manageable phase shift, the incident signal is controlled by each element in the RIS. To achieve the phase alignment of the signals, RIS adjusts the phase shifts of all the elements from different transmission paths at a desired receiver, which is so-called as passive beamforming, and hence improving the achievable rate and the signal energy [5], [6]. Besides, another advantage is that the RIS exhibits capability of a full-duplex mode without complex interference cancellation approaches.

The beamforming design for IRS-empowered wireless networks has recently attracted considerable attention [7], [8]. The base station (BS) transmit power minimization problem was considered in [7] by jointly optimizing active beamforming at the BS and passive beamforming at the IRS. It was demonstrated that the IRS can significantly reduce the energy consumption in wireless networks [7]. The achievable maximin data rate optimization problem was considered in [8] via random matrix theory. The authors in [9] provided an approximation computations of the achievable data rate by evaluating the performance of an uplink RIS assisted communication system, and determine the effect of limited phase shifts on the data rate. The study in [10] introduced the concept of RIS-assisted communications employing index modulation (IM) such as RIS-spatial modulation (RIS-SM) and RIS-space shift keying (RIS-SSK) schemes. These two schemes are reported as the spectral efficiency improvement by utilization of the IM principle for the indices of multiple receive antennas. Regarding promising applications, references [11] explored RIS relying on an unmanned aerial vehicle (UAV). In particular, the authors conducted design of passive beamforming of RIS antenna elements to minimize the total decoding error rate and find the UAV's optimal position. The authors applied non-linear and non-convex optimization to address performance improvement. In [12], an RIS-enhanced multiple-input single-output (MISO) system as well as reflection pattern modulation (RPM) are studied. The authors examined the joint active and passive beamforming which is carefully designed by computing the communication outage probability. They introduced expression of an optimization problem to maximize the average received signal power by jointly optimizing the active beamforming at the access point (AP) and passive beamforming at the RIS.

To support multiple users and provide the maximization of sumrate and energy efficiency, the authors of [5], [13], [14] considered an RIS-assisted downlink transmission scenario. Reference [14] presented multi-user multiple antennas system by design the transmit powers per user and the values for the surface elements that jointly maximize the system's energy efficiency performance. Recently, the interesting problem of energy and spectrum efficiency are investigated in [15] and [16]. In [15], they considered energy harvesting adapted in RIS to maximize the average energy efficiency by enabling a BS to determine the transmit power and RIS configuration, under uncertainty on the wireless channel and harvested energy of the RIS system. Reference [16] evaluated two-way communications via RIS where two users communicate through a common RIS. Further, they computed a gamma approximation to model a product of Rayleigh random variables, and then the approximate expressions are computed in terms of the outage probability and the average throughput. Even more recently, design of sparse channel sensors is conducted on RIS architectures [17], in which several existing RIS units are active, and RIS-assisted physical-layer security schemes [18]. In the other line of research, the calculation of average symbol error probability (SEP) is presented for performance evaluation of RIS-assisted systems [19]. Reference [20] evaluated secure multicast transmission with the deployment of RIS. In the impact of a single-antenna eavesdropper, a multiple-antennas transmitter multicasts the common signals to a group of single-antenna receivers, in which a RIS is set up to suppress the signals for the eavesdropper and improve the desired signals for the receivers.

As another approach to improve spectrum efficiency, non-Orthogonal Multiple Access (NOMA) [21]–[25] is developed along with its promising applications regarding wireless access technique for the coming 5G era. In the principle, at the transmitter, NOMA employs non-orthogonal transmission and superimpose users' signal in power domain for higher spectrum efficiency. NOMA can serve multiple users over the same resource block which is different from Orthogonal Multiple Access (OMA), thus it can effectively improve sum rate. Together with improvements in the transmitter, the receiver needs successive interference cancellation (SIC) adopted to decode the users' signal. Specifically, one can decode the user with the best channel condition firstly, while other users are recognized as interference. References [23-27] gave the promising applications of NOMA and system performance is analysed. NOMA can further improve spectrum efficiency (SE) due to non-orthogonal transmission and SIC, thus the application of NOMA to cognitive radio (CR) network is necessary to improve the SE in CR-NOMA network. The authors in [24] proposed model to improve the performance of far users. In particular, partial relay selection architecture is adopted at relay using full-duplex (FD) and half duplex (HD) modes for both uplink and downlink communications. For in-depth performance evaluation, they derived the closed-form expressions of the outage probabilities of the users in FD and HD for relay-aided CR-NOMA networks. Reference [26] designed a CR-NOMA model and an SE optimization problem was solved by optimizing the sensing subslot. Since CR-NOMA combines the advantages of both the techniques, it is considered as a promising technique for the coming 5G communication system [27].

A. RELATED WORK

The deployment of next generation multi-user communication systems based on RIS has been faced a number of challenges. Firstly, the limited spectrum available to

RIS-based systems limits the number of users that can be served simultaneously. Secondly, the orthogonal multiple access (OMA) schemes used in conventional wireless systems are highly susceptible to interference among users. To enable capable of serving a large number of users in the same resource block, NOMA schemes multiplex signals in domains rather than frequency or time, and thus providing a massive number of connections. Nonetheless, there has been very little research on the integration of RIS with NOMA. For example, the authors in [28] explored a system designed by examining the passive beamforming weights at the RIS to serve paired power-domain NOMA users. Motivated by the potential joint advantages of RISs and NOMA networks, this study considered the outage performance of a RIS-aided NOMA for downlink, where two transmission schemes are considered, and hence the spectrum efficiency could be improved. Reference [29] studied the problem of joint deployment of phase shift design and power allocation in the context of multiple-input single-output (MISO) NOMA network. The authors also formulated expressions for maximizing the energy efficiency with considering users particular data requirements. The authors in [30] designed a novel passive beamforming weight at RISs in a multiple-input multiple-output (MIMO) NOMA network for simultaneously serving paired users. They derived the closed-form formulas both for the outage probability and for the ergodic rate. The diversity orders as well as the high signal-to-noise-ratio (SNR) slopes are considered for engineering insights. In [31], the authors explored RIS assisted wireless communication system with rate splitting multiple access (RSMA). In this network, the authors maximized the energy efficiency performance of the network by controlling the phase shifts of the RIS and beamforming of the base station. In [32], the authors derived the probability of a backscatter channel dominating the composite channel as a performance measure to determine the number of reflectors in RIS required for a given system.

B. CONTRIBUTIONS

In this paper, different from [28]–[32], we first assume that RIS allows reflecting signal and send its own signal to destinations (this is possible when backscatter function is enabled). It is assumed that perfect CSI is available to study the ultimate performance of the RIS-aided NOMA systems. The formulated problem exhibits mathematically derivations for main system metrics. Furthermore, the benchmark model of RIS using OMA is compared, and the improvement of RIS is explored.

The main contributions of this work are summarized as follows:

- Firstly, this paper considers an downlink cellular network where the RIS and direct links between the base station (BS) and the users get more benefits from the function of backscatter to enable NOMA transmission. The RIS-aided NOMA architecture is used to ensure that additional cell-edge user can also be served instead of normal operation of near users associated with the BS which has limited number of serving users. Such benefit can be achieved by allocating different power levels to users.
- Secondly, to evaluate advantages of RIS, this paper is one of the early attempts to study the performance system metrics such as outage probability, ergodic capacity and throughput for the RIS-aided NOMA systems. We realize that the system metrics mostly depend on the number of reflecting elements in the RIS. Therefore, we present two methods to compute main metric, i.e. outage probability.
- Finally, the system compassion with the RIS employing OMA is also investigated. Numerical results verify that the proposed RIS-aided NOMA systems outperform than RIS relying OMA in term of outage performance, while the ergodic capacity in the considered system using NOMA is better than that of OMA at specific power allocation factor assigned to user. Interestingly, the existence of optimal outage performance of the near user at given number of reflecting elements in RIS and given transmit SNR at the BS.

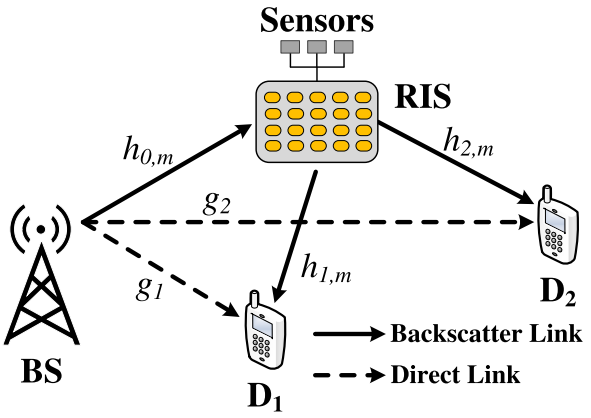

FIGURE 1. System model of backscatter RIS relying on NOMA.

The rest of this paper is summarized as follows. Section II introduces the architecture of RIS-aided wireless communication system model relying NOMA and the problem formulation of outage probability. In Section III, the derivations of outage probability for two users in NOMA mode are briefly introduced. The counterpart, RIS relying on OMA, is explored, and, then throughput is encountered. The ergodic capacity is examined in Section IV. Section V presents simulation results to exhibit the performance metrics of the proposed systems. Finally, our study is concluded in Section VI.

II. SYSTEM ARCHITECTURE

As depicted in Fig. 1, the considered system includes of a backscatter link, direct link, one BS, one RIS and the near user D_1, the far user D_2. We design RIS unit with m passive reflectors ($m = 1, 2, \ldots, M$). Further, it is required a controller

TABLE 1. Key parameters of the system model.

Symbols	Description
a_i	The power allocation coefficient with $i \in \{1,2\}$, $a_1 + a_2 = 1$ and $a_1 < a_2$
P_S	The transmit power at the BS
n_i	The AWGN noise term followed $\mathcal{CN}(0, N_0)$
x_i	The information of D_i
R_i	The target rate at D_i
α	The path loss exponent
β	the RIS attenuation coefficient
θ_m	The adjustable phase produced by the $m = [1, \ldots, M]$ reflecting element of RIS.
$h_{0,m}$	The channel link between BS and RIS
$h_{1,m}$	The channel link between RIS and D_1
$h_{2,m}$	The channel link between RIS and D_2
g_1	The channel link between BS and D_1
g_2	The channel link between BS and D_2
$Pr\{\cdot\}$	Probability operator
$E\{\cdot\}$	Expectation operator
$f_X(\cdot)$	Probability density function (PDF) of the Random Variable (RV) X
$F_X(\cdot)$	Cumulative distribution function (CDF) of RV X
$K_a(\cdot)$	Modified Bessel function of the second kind and order a
$Ei(-x)$	Exponential integral function: $Ei(-x) = \int_{-\infty}^{x} e^p p^{-1} dp$
$G_{p,q}^{m,n}[.]$	Meijer G-function given in [37, Eq. (9.301)]

to achieve channel state information (CSI) acquisition and information transmission [32]. We denote channels for links BS-RIS, RIS-D_1, RIS-D_2, BS-D_1, BS-D_2 as $h_{0,m}$, $h_{1,m}$, $h_{2,m}$, g_1, g_2 respectively which correspond to distance $d_{h_0}, d_{h_1}, d_{h_2}$, d_{g_1}, d_{g_2}. It is assumed all fading channels are independent and considered transmission time falls within a coherence interval of the channel). It is noted that $y \sim \mathcal{CN}(0, a)$ means that y is a complex normal distributed random variable with zero mean and variance a. The other main parameters can reported in Table 1.

In the k–th time slot, the BS communicate with other nodes using a superimposed message targeting to users D_1 and D_2 as below [1]

$$x[k] = \sqrt{a_1 P_S} x_1[k] + \sqrt{a_2 P_S} x_2[k], \tag{1}$$

where a_1 and a_2 stand for the portion of powers allocated for D_1 and D_2 signals, respectively, and satisfying constraint $a_1 < a_2$ and $a_1 + a_2 = 1$. The received signal at user $D_i, i \in \{1,2\}$ can be given by [2]

$$y_i[k] = \frac{g_i x[k]}{\sqrt{d_{g_i}^{\alpha}}} + \beta \sum_{m=1}^{M} \frac{h_{0,m} h_{i,m} e^{j\theta_m} x[k] s[k]}{\sqrt{d_{h_0}^{\alpha} d_{h_i}^{\alpha}}} + n_i[k], \tag{2}$$

where β is called as the RIS attenuation coefficient, α is path-loss exponent and $n_i[k]$ is additive white Gaussian noise with variance N_0. It is worth noting that $s[k]$ is backscatter signal.[3] It is noted that in (2), $\theta_m \in [0, 2\pi)$ is the adjustable phase produced by the m-th reflecting element of RIS. It is worth noting that M meta-suface elements of the RIS are located closely, then the distances from all meta-suface to each user are same $d_{h_i} = \left[d_{h_{i,m}}, \ldots, d_{h_{i,M}}\right], i \in \{1,2\}$.

Due to $\left|\sum_{m=1}^{M} h_{0,m} h_{i,m} e^{j\theta_m}\right| = \sum_{m=1}^{M} \left|h_{0,m}\right| \left|h_{i,m}\right|$, $i \in \{1,2\}$ in the case of perfect CSI [32], let us define variable $T_{b,i} \triangleq \sum_{m=1}^{M} \left|h_{0,m}\right| \left|h_{i,m}\right|$ and variable $G_i \triangleq |g_i|$. We first calculate signal-to-interference-plus-noise ratio (SINR) to detect D_2's signal at user D_1 as [28]

$$\bar{\gamma}_{2\to 1} = \frac{\rho a_2 \left|\tilde{T}_1\right|^2}{\rho a_1 \left|\tilde{T}_1\right|^2 + 1}, \tag{3}$$

where $\left|\tilde{T}_1\right|^2 \triangleq \beta^2 d_{h_0}^{-\alpha} d_{h_1}^{-\alpha} T_{b,1}^2 + G_1^2 d_{g_1}^{-\alpha}$ and $\rho = P_S / N_0$ is the transmit signal-to-noise radio (SNR) at the BS. Note that s, x_1 and x_2 are supposed to be normalized unity power signals, i.e, $E\{s^2\} = E\{x_1^2\} = E\{x_2^2\} = 1$ in which $E\{\cdot\}$ is the expectation operator.

[1] As considerations in references [22]–[27], the case of more than two NOMA users in wireless system results in worse performance, in this manner we design many group of users. Such user group should be contain two users for better system performance and thus we only consider performance of two users.

[2] Normally, as references [28]–[31], they did not research on capable of backscatter signals from RIS, which limits benefit of RIS. In this paper, backscatter links add more signals from RIS to serve NOMA users.

[3] It is noteworthy that backscatter-assisted RIS-NOMA system can increase the range of the communication by utilizing RIS. This mechanism provides more benefits to the current RIS system or normal backscatter system where the tag and the reader should be located in short distances from each other to reduce severe phase distortion of the channel associated with multipath propagation [37].

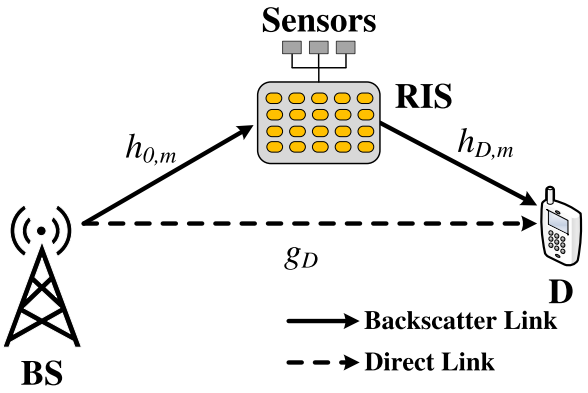

FIGURE 2. System model of backscatter RIS relying on OMA.

Performing SIC at user D_1 using the principle of NOMA, user D_1, D_2 can detect its signal by calculating SINR as

$$\bar{\gamma}_1 = \rho a_1 \left|\tilde{T}_1\right|^2. \tag{4}$$

Next, the SINR at D_2 to detect its own signal can be expressed as

$$\bar{\gamma}_2 = \frac{\rho a_2 \left|\tilde{T}_2\right|^2}{\rho a_1 \left|\tilde{T}_2\right|^2 + 1}, \tag{5}$$

where $\left|\tilde{T}_2\right|^2 \triangleq \beta^2 d_{h_0}^{-\alpha} d_{h_2}^{-\alpha} T_{b,2}^2 + G_2^2 d_{g_2}^{-\alpha}$.

Different from NOMA architecture, in Fig. 2, only user D is examined in term of system performance. In this case, the BS transmit signal targets directly to one destination. It is worth that if we want to send to two continuous signals x_1, x_2, we need more time slots to achieve same job as the case of RIS relying on NOMA.

The received signal that user D can get as

$$y_D[k] = \sqrt{P_S}\left(\beta \sum_{m=1}^{M} \frac{h_{0,m} h_{D,m} e^{j\theta_m}}{\sqrt{d_{h_0}^{\alpha} d_{h_D}^{\alpha}}} + \frac{g_D}{\sqrt{d_{g_D}^{\alpha}}}\right) x_S[k] + n_D[k], \tag{6}$$

where n_D is AWGN noise term.

In this circumstance, the received SNR at D can be given as

$$\begin{aligned}\bar{\gamma}_D &= \rho \left| \frac{|g_D|}{\sqrt{d_{g_D}^{\alpha}}} + \beta \sum_{m=1}^{M} \frac{\left|h_{0,m} h_{D,m}\right| e^{j\theta_m}}{\sqrt{d_{h_0}^{\alpha} d_{h_D}^{\alpha}}} \right|^2 \\ &= \rho \left[|g_D|^2 d_{g_D}^{-\alpha} + \beta^2 d_{h_0}^{-\alpha} d_{h_D}^{-\alpha} \left|h_{0,m} h_{D,m}\right|^2 \right]. \end{aligned} \tag{7}$$

Remark 1: Regarding computation related to the backscatter link in (3), (5), and (7), this paper intends to introduce interesting system to achieve more benefits compared conventional RIS systems [28]–[32]. By sending signal from RF source, the backscatter link is also called multiplicative multiple access channel, and with the assistance of RIS, two enablers are joint proceed for transmitting RF source regarding information processing. However, more complicated deployment of RIS need be required to enhance the communication compare with transmitting base station's own information to the receivers. Therefore, it is wise to strengthen the transmissions from backscatter and normal RIS links and such hybrid scheme might have higher cost in term of hardware design. However, this regard is out of scope of our current study.

III. OUTAGE PROBABILITY (OP) ANALYSIS

This section focuses on presenting the theoretical framework for the performance analysis of the RIS-aided NOMA system and the counterpart, namely RIS-OMA. In particular, wireless channel characteristic and component in the RIS are two main factors affecting to performance metrics in the RIS-aided NOMA wireless systems, in which the improvement at specific parameters are expected.

In the subsequent sections, we consider main metric (outage probability) through two methods which are decided by how large the number of RIS meta-suface elements is.

A. RIS-NOMA WITH DIRECT LINK

In case of large M, we examine OP performance as below. As a main performance metric, OP is defined that capability to transmit signal with SINR less than the threshold. These SINR thresholds are $\varepsilon_2 = 2^{2R_2} - 1$ and $\varepsilon_1 = 2^{2R_1} - 1$ with R_1, R_2 are denoted as the target rates for users D_1, D_2 to detect x_1 and x_2, respectively. In particular, the OP at user D_2 is expressed by [4]

$$\begin{aligned}\mathcal{OP}_2 &= Pr\left(\bar{\gamma}_2 < \varepsilon_2\right) \\ &= Pr\left(\beta^2 d_{h_0}^{-\alpha} d_{h_2}^{-\alpha} T_{b,2}^2 + d_{g_2}^{-\alpha} T_2^2 < \theta_2\right) \\ &= Pr\left(T_2^2 < \frac{\theta_2 - \beta^2 d_{h_0}^{-\alpha} d_{h_2}^{-\alpha} T_{b,2}^2}{d_{g_2}^{-\alpha}}, T_{b,2}^2 < \frac{\theta_2}{\beta^2 d_{h_0}^{-\alpha} d_{h_2}^{-\alpha}}\right) \\ &= \int_0^{\frac{\theta_2}{\beta^2 d_{h_0}^{-\alpha} d_{h_2}^{-\alpha}}} f_{T_{b,2}^2}(y) \int_0^{\frac{\theta_2 - \beta^2 d_{h_0}^{-\alpha} d_{h_2}^{-\alpha} y}{d_{g_2}^{-\alpha}}} f_{T_2^2}(z) dy dz, \end{aligned} \tag{8}$$

where $\theta_2 = \frac{\varepsilon_2}{\rho(a_2 - a_1\varepsilon_2)}$ and $Pr(\cdot)$ is the probability operator.

In case of large M, we find that $\sum_{m=1}^{M} h_{0,m} h_{i,m} \sim \mathcal{CN}(0, M)$ and $g_i \sim \mathcal{CN}(0, 1)$, the PDF of channel $T_{b,i}$ and G_i, i.e. $f_{G_i^2}(x)$ and $f_{T_{b,i}^2}(x)$ are given by [32]

$$f_{G_i^2}(x) = e^{-x}, \tag{9a}$$

$$f_{T_{b,i}^2}(x) = \frac{1}{M} e^{-\frac{x}{M}}. \tag{9b}$$

[4] Although reference [33] studied the impact of two phase shifting designs, namely coherent phase shifting and random discrete phase shifting, on the performance of RIS-assisted NOMA, we design newer system model and present closed-form expressions for outage performance in different manner. Our results would benefit to evaluate RIS-NOMA, especially indicate performance among two users. We also find optimal outage performance for specific user in numerical simulation section.

Now, with (9a) and (9b), such outage performance can be evaluated as

$$\begin{aligned}\mathcal{OP}_2 &= \frac{1}{M}\int_0^{\frac{\theta_2}{\beta^2 d_{h_0}^{-\alpha} d_{h_2}^{-\alpha}}} e^{-\frac{y}{M}}\left(1-e^{-\frac{\theta_2-\beta^2 d_{h_0}^{-\alpha} d_{h_2}^{-\alpha} y}{d_{g_2}^{-\alpha}}}\right)dy \\ &= \left(1-e^{-\frac{\theta_2}{M\beta^2 d_{h_0}^{-\alpha} d_{h_2}^{-\alpha}}}\right) - \frac{e^{-\frac{\theta_2}{d_{g_2}^{-\alpha}}}}{M} \\ &\quad\times \int_0^{\frac{\theta_2}{\beta^2 d_{h_0}^{-\alpha} d_{h_2}^{-\alpha}}} e^{-y\left(\frac{1}{M}-\frac{\beta^2 d_{h_0}^{-\alpha} d_{h_2}^{-\alpha}}{d_{g_2}^{-\alpha}}\right)}dy \\ &= 1-e^{-\frac{\theta_2}{M\beta^2 d_{h_0}^{-\alpha} d_{h_2}^{-\alpha}}} - \frac{d_{g_2}^{-\alpha} e^{-\frac{\theta_2}{d_{g_2}^{-\alpha}}}}{\left(d_{g_2}^{-\alpha}-M\beta^2 d_{h_0}^{-\alpha} d_{h_2}^{-\alpha}\right)} \\ &\quad\times\left[1-e^{-\frac{\theta_2}{\beta^2 d_{h_0}^{-\alpha} d_{h_2}^{-\alpha}}\left(\frac{1}{M}-\frac{\beta^2 d_{h_0}^{-\alpha} d_{h_2}^{-\alpha}}{d_{g_2}^{-\alpha}}\right)}\right]. \end{aligned} \tag{10}$$

In the next step, we have higher priority to consider worse case of perfect SIC for the OP for user D_1, which is denoted as $\mathcal{OP}_1$ and it can be computed by

$$\begin{aligned}\mathcal{OP}_1 &= Pr\left(\bar{\gamma}_{2\to 1} < \varepsilon_2 \cup \bar{\gamma}_1 < \varepsilon_1\right) \\ &= Pr\left(\left|\tilde{T}_1\right|^2 < \theta_{\max}\right). \end{aligned} \tag{11}$$

where $\theta_{\max} = \max\left(\frac{\varepsilon_2}{\rho(a_2-a_1\varepsilon_2)}, \frac{\varepsilon_1}{\rho a_1}\right)$.

Similarly with performance of user D_2, solving of $\mathcal{OP}_1$ benefits to evaluation for performance of user D_1. In particular, it can be achieved $\mathcal{OP}_1$ as

$$\begin{aligned}\mathcal{OP}_1 &= 1-e^{-\frac{\theta_{\max}}{M\beta^2 d_{h_0}^{-\alpha} d_{h_1}^{-\alpha}}} - \frac{d_{g_1}^{-\alpha} e^{-\frac{\theta_{\max}}{d_{g_1}^{-\alpha}}}}{\left(d_{g_1}^{-\alpha}-M\beta^2 d_{h_0}^{-\alpha} d_{h_1}^{-\alpha}\right)} \\ &\quad\times\left[1-e^{-\frac{\theta_{\max}}{\beta^2 d_{h_0}^{-\alpha} d_{h_1}^{-\alpha}}\left(\frac{1}{M}-\frac{\beta^2 d_{h_0}^{-\alpha} d_{h_1}^{-\alpha}}{d_{g_1}^{-\alpha}}\right)}\right]. \end{aligned} \tag{12}$$

Remark 2: From our results in (10), (12), these formulas of outage behavior depend on lots of parameters. However, since the SNR at source and the number of elements in RIS has higher weights, the outage performance is predicted to be adjusted by controlling M and ρ. Further parameters can be evaluated in numerical simulation section.

B. RIS-NOMA WITHOUT DIRECT LINK

In the case of smaller M, we cannot find tractable solution to provide explicit analysis for the considered system illustrated in previous section. Fortunately, to robust benefit of RIS and consider in main link (BS- RIS- users), we present other way to compute outage probability for two NOMA users. In particular, the received signals at user D_1 and user D_2 are expressed respectively by [36]

$$y_i[k] = \frac{\beta}{\sqrt{d_{h_0}^{\alpha} d_{h_i}^{\alpha}}}\mathbf{h}_0^H \Theta \mathbf{h}_i x[k] + n_i, \quad i \in \{1,2\} \tag{13}$$

where $(\cdot)^H$ is represented as the conjugate-transpose operation. Due to matrix based computation, we denote the complex channel coefficient between the BS and RIS, and between the RIS and two users are denoted as $\mathbf{h}_0 \in \mathbb{C}^{M\times 1}$ and $\mathbf{h}_i \in \mathbb{C}^{M\times 1}$, respectively. $\Theta = diag\left(e^{j\theta_1}, \ldots, e^{j\theta_m}, \ldots, e^{j\theta_M}\right)$ stands for a diagonal matrix, $diag(\cdot)$ iss a diagonal matrix.

Similar from the first method, the SINR for the user D_1 used to decode the D_2's signal is expressed by

$$\Gamma_{2\to 1} = \frac{\rho a_2 \beta^2 d_{h_0}^{-\alpha} d_{h_1}^{-\alpha}\left|\mathbf{h}_0^H \Theta \mathbf{h}_1\right|^2}{\rho a_1 \beta^2 d_{h_0}^{-\alpha} d_{h_1}^{-\alpha}\left|\mathbf{h}_0^H \Theta \mathbf{h}_1\right|^2 + 1}. \tag{14}$$

By conducting SIC, the user D_1 eliminates interference from signal x_2, then it decodes its signal by computing the SNR as

$$\Gamma_1 = \rho a_1 \beta^2 d_{h_0}^{-\alpha} d_{h_1}^{-\alpha}\left|\mathbf{h}_0^H \Theta \mathbf{h}_1\right|^2. \tag{15}$$

Similarly, the SINR at D_2 is computed to detect its own signal x_2 as

$$\Gamma_2 = \frac{\rho a_2 \beta^2 d_{h_0}^{-\alpha} d_{h_2}^{-\alpha}\left|\mathbf{h}_0^H \Theta \mathbf{h}_2\right|^2}{\rho a_1 \beta^2 d_{h_0}^{-\alpha} d_{h_2}^{-\alpha}\left|\mathbf{h}_0^H \Theta \mathbf{h}_2\right|^2 + 1}. \tag{16}$$

To enable the second method, 1-bit coding scheme is acquired to achieve the discrete amplitude/phase shift modes for RIS-NOMA networks. In this regard, the elements of diagonal matrix Θ are replaced with 0 or 1. Compare with the first method, the second method exhibits as cost-effective solution due to the smaller number of meta-surface elements.

To further compute such SINRS, we define $\mathbf{V} = \mathbf{I_P} \otimes \mathbf{1_{M/P}}$, where $\mathbf{1_{M/P}}$ is a column vector of all ones with $M/P \times 1$. The $p-th$ column of $\mathbf{V}$ is denoted by $\mathbf{v}_p$ with $M \times 1$ and $\mathbf{v}_p^H \mathbf{v}_l = 0$ for $p \neq l$. Therefore, by randomly choosing $\mathbf{v}_p$, the SINRs of (14), (15) and (16) with 1-bit coding are maximized as

$$\tilde{\Gamma}_{2\to 1} = \max_{\mathbf{v}_p} \frac{\rho a_2 \beta^2 d_{h_0}^{-\alpha} d_{h_1}^{-\alpha}\left|\mathbf{v}_p^H \mathbf{D}_1 \mathbf{h}_0\right|^2}{\rho a_1 \beta^2 d_{h_0}^{-\alpha} d_{h_1}^{-\alpha}\left|\mathbf{v}_p^H \mathbf{D}_1 \mathbf{h}_0\right|^2 + 1}, \tag{17a}$$

$$\tilde{\Gamma}_1 = \max_{\mathbf{v}_p} \rho a_1 \beta^2 d_{h_0}^{-\alpha} d_{h_1}^{-\alpha}\left|\mathbf{v}_p^H \mathbf{D}_1 \mathbf{h}_0\right|^2, \tag{17b}$$

$$\tilde{\Gamma}_2 = \max_{\mathbf{v}_p} \frac{\rho a_2 \beta^2 d_{h_0}^{-\alpha} d_{h_1}^{-\alpha}\left|\mathbf{v}_p^H \mathbf{D}_2 \mathbf{h}_0\right|^2}{\rho a_1 \beta^2 d_{h_0}^{-\alpha} d_{h_1}^{-\alpha}\left|\mathbf{v}_p^H \mathbf{D}_2 \mathbf{h}_0\right|^2 + 1}, \tag{17c}$$

where $\mathbf{D}_1$ and $\mathbf{D}_2$ are the diagonal matrix with its diagonal elements obtained from channel matrices $\mathbf{h}_1$ and $\mathbf{h}_2$.

The PDF of $\left|\mathbf{v}_p^H \mathbf{D}_i \mathbf{h}_0\right|^2$, $i \in \{1,2\}$ can be expressed as [37]

$$f_{\left|\mathbf{v}_p^H \mathbf{D}_1 \mathbf{h}_0\right|^2}(x) = \frac{2}{\Gamma\left(\frac{M}{P}\right)} x^{\frac{\frac{M}{P}-1}{2}} K_{\frac{M}{P}-1}\left(2\sqrt{x}\right). \tag{18}$$

Considering outage behavior occurred at the user D_1, since it fails to detect both the D_2's signal x_2 and signal x_1. In particular, such OP is given by

$$\begin{aligned}\mathcal{OP}_{1,nodir} &= \prod_{p=1}^{P} \Pr\left(\tilde{\Gamma}_{2\to 1} < \varepsilon_2 \cup \tilde{\Gamma}_1 < \varepsilon_1\right) \\ &= \left[\Pr\left(\left|\mathbf{v}_p^H \mathbf{D}_1 \mathbf{h}_0\right|^2 < \varpi_{\max}\right)\right]^P, \end{aligned} \tag{19}$$

where $\varpi_2 = \frac{\varepsilon_2}{\rho(a_2 - a_1\varepsilon_1)\beta^2 d_{h_0}^{-\alpha} d_{h_1}^{-\alpha}}$, $\varpi_1 = \frac{\varepsilon_1}{\rho a_1 \beta^2 d_{h_0}^{-\alpha} d_{h_1}^{-\alpha}}$ and $\varpi_{\max} = \max(\varpi_1, \varpi_2)$.

Proposition 1: The closed-form expression of the OP at user D_1 can be formulated by

$$\mathcal{OP}_{1,nodir} = \left[1 - \frac{2(\varpi_{\max})^{\frac{M}{2P}}}{\Gamma\left(\frac{M}{P}\right)} K_{\frac{M}{P}}\left(2\sqrt{\varpi_{\max}}\right)\right]^P. \tag{20}$$

Proof 1: See Appendix A

Similar to solving of $\mathcal{OP}_{1,nodir}$, the OP at user D_2 can be computed by

$$\begin{aligned}\mathcal{OP}_{2,nodir} &= \prod_{p=1}^{P} \Pr\left(\tilde{\Gamma}_2 < \varepsilon_2\right) \\ &= \left[1 - \frac{2(\bar{\varpi}_2)^{\frac{M}{2P}}}{\Gamma\left(\frac{M}{P}\right)} K_{\frac{M}{P}}\left(2\sqrt{\bar{\varpi}_2}\right)\right]^P, \end{aligned} \tag{21}$$

where $\bar{\varpi}_2 = \frac{\varepsilon_2}{\rho(a_2 - a_1\varepsilon_1)\beta^2 d_{h_0}^{-\alpha} d_{h_2}^{-\alpha}}$.

In the consequent sections, we only focus on the first method to further examine other system metrics.

C. THE BENCHMARK CASE: OMA

From result reported in (7), the OP can be expressed as follows

$$\begin{aligned}\mathcal{OP}_D &= \Pr\left(\tilde{\gamma}_D < \varepsilon_0\right) \\ &= \Pr\left(G_D^2 < \frac{\varepsilon_0}{d_{g_D}^{-\alpha}\rho} - \frac{\ell_d T_{b,D}^2}{d_{g_D}^{-\alpha}}, T_{b,D}^2 < \frac{\varepsilon_0}{\ell_d \rho}\right) \\ &= \int_0^{\chi} f_{T_{b,D}^2}(x) \int_0^{\frac{\varepsilon_0}{d_{g_D}^{-\alpha}\rho} - \frac{\ell_d x}{d_{g_D}^{-\alpha}}} f_{G_D^2}(y) dx dy, \end{aligned} \tag{22}$$

where $G_D \triangleq |g_D|$, $T_{b,D} \triangleq \sum_{m=1}^{M} \left|h_{0,m} h_{D,m}\right|$, $\varepsilon_0 = 2^{4R_0} - 1$, $\chi = \frac{\varepsilon_0}{\ell_d \rho}$ and $\ell_d = \beta^2 d_{h_0}^{-\alpha} d_{h_D}^{-\alpha}$.

Similar to solving of (10) and after some manipulation, this can be achieved $\mathcal{OP}_D$ as

$$\begin{aligned}\mathcal{OP}_D &= \frac{1}{M} \int_0^{\chi} e^{-\frac{x}{M}} \left(1 - e^{-\frac{\varepsilon_0}{d_{g_D}^{-\alpha}\rho} + \frac{\ell_d x}{d_{g_D}^{-\alpha}}}\right) dx \\ &= \left(1 - e^{-\frac{\chi}{M}}\right) - \frac{d_{g_D}^{-\alpha} e^{-\frac{\varepsilon_0}{d_{g_D}^{-\alpha}\rho}}}{\left(d_{g_D}^{-\alpha} - M\ell_d\right)} \left(1 - e^{-\chi\left(\frac{1}{M} - \frac{\ell_d}{d_{g_D}^{-\alpha}}\right)}\right). \end{aligned} \tag{23}$$

D. SYSTEM THROUGHPUT ANALYSIS

Although OP is known as main performance metric, throughput can demonstrate performance at fixed rate in delay-limited transmission mode. Such throughput for two users in RIS-NOMA and RIS-OMA can be given respectively as

$$\tau_{NOMA}^{\iota} = (1 - \mathcal{OP}_{\iota}) R_{\iota}, \quad \iota \in \{1, 2\} \tag{24a}$$

$$\tau_{OMA} = (1 - \mathcal{OP}_D) R_0. \tag{24b}$$

E. THE APPROXIMATION OF OUTAGE PROBABILITY

In this section, we provide approximate computation of outage probability. In particular, based on analytical result in (11), when $\rho \to \infty$, the asymptotic outage probability of D_2 for RIS NOMA with $e^{-x} \approx 1 - x$ is given by

$$\begin{aligned}\mathcal{OP}_2^{\infty} &= \frac{\theta_2}{M\beta^2 d_{h_0}^{-\alpha} d_{h_2}^{-\alpha}} - \frac{1}{\left(d_{g_2}^{-\alpha} - M\beta^2 d_{h_0}^{-\alpha} d_{h_2}^{-\alpha}\right)} \\ &\quad \times \left(d_{g_2}^{-\alpha} - \theta_2\right) \frac{\theta_2}{\beta^2 d_{h_0}^{-\alpha} d_{h_2}^{-\alpha}} \left(\frac{1}{M} - \frac{\beta^2 d_{h_0}^{-\alpha} d_{h_2}^{-\alpha}}{d_{g_2}^{-\alpha}}\right). \end{aligned} \tag{25}$$

Based on (13) and (15), the asymptotic outage probability of D_1 for RIS NOMA and D for RIS OMA are given as

$$\begin{aligned}\mathcal{OP}_1^{\infty} &= \frac{\theta_{\max}}{M\beta^2 d_{h_0}^{-\alpha} d_{h_1}^{-\alpha}} - \frac{1}{\left(d_{g_1}^{-\alpha} - M\beta^2 d_{h_0}^{-\alpha} d_{h_1}^{-\alpha}\right)} \\ &\quad \times \left(d_{g_1}^{-\alpha} - \theta_{\max}\right) \frac{\theta_{\max}}{\beta^2 d_{h_0}^{-\alpha} d_{h_1}^{-\alpha}} \left(\frac{1}{M} - \frac{\beta^2 d_{h_0}^{-\alpha} d_{h_1}^{-\alpha}}{d_{g_1}^{-\alpha}}\right). \end{aligned} \tag{26}$$

and

$$\begin{aligned}\mathcal{OP}_D^{\infty} &= \frac{\chi}{M} - \frac{1}{\left(d_{g_D}^{-\alpha} - M\ell_d\right)} \\ &\quad \times \left(d_{g_D}^{-\alpha} - \frac{\varepsilon_0}{\rho}\right) \chi \left(\frac{1}{M} - \frac{\ell_d}{d_{g_D}^{-\alpha}}\right). \end{aligned} \tag{27}$$

Next, we would provide more insights by introducing the diversity orders for users D_1, D_2 and D, which can be defined as [36, Eq. (13)]

$$d_v = -\underbrace{lim}_{\rho\to\infty} \frac{\log_{10}\left(\mathcal{OP}_v^{\infty}\right)}{\log_{10}(\rho)}, v \in \{1, 2, D\}. \tag{28}$$

Remark 3: It is straightforward to find the diversity orders of D_1, D_2 and D as $d_1 = d_2 = d_D = M$, respectively. Although some factors make influence on the outage performance of users, however in high SNR region, system performance does not rely any factors. It is expected to verify such a finding in numerical simulation section.

IV. ERGODIC CAPACITY ANALYSIS

The following propositions return two equivalent and novel closed-form expressions to consider ergodic capacity for users in such RIS-NOMA systems. We also examine ergodic capacity for RIS-OMA as necessary comparison.

A. NOMA

First, the ergodic capacity at D_2 for NOMA is calculated as

$$\mathcal{C}_2 \triangleq E\left\{\frac{1}{2}\log_2\left(1+\bar{\gamma}_2\right)\right\}. \tag{29}$$

Proposition 2: The closed-form expression of ergodic capacity at user D_2 can be given by

$$\mathcal{C}_2 = \frac{1}{2\ln 2}\left[\bar{\mathcal{A}}_1 + \frac{d_{g_2}^{-\alpha}}{\left(d_{g_2}^{-\alpha} - M\beta^2 d_{h_0}^{-\alpha} d_{h_2}^{-\alpha}\right)}\left(\bar{\mathcal{A}}_2 - \bar{\mathcal{A}}_3\right)\right], \tag{30}$$

where

$$\bar{\mathcal{A}}_1 = \left[G_{1,2}^{2,1}\left(\frac{\nu}{\rho\left(a_2+a_1\right)}\middle|\begin{matrix}0\\0,0\end{matrix}\right) - G_{1,2}^{2,1}\left(\frac{\nu}{\rho a_1}\middle|\begin{matrix}0\\0,0\end{matrix}\right)\right], \tag{31a}$$

$$\bar{\mathcal{A}}_2 = \left[G_{1,2}^{2,1}\left(\frac{d_{g_2}^{\alpha}}{\rho\left(a_2+a_1\right)}\middle|\begin{matrix}0\\0,0\end{matrix}\right) - G_{1,2}^{2,1}\left(\frac{d_{g_2}^{\alpha}}{\rho a_1}\middle|\begin{matrix}0\\0,0\end{matrix}\right)\right], \tag{31b}$$

$$\bar{\mathcal{A}}_3 = \left[G_{1,2}^{2,1}\left(\frac{\psi}{\rho\left(a_2+a_1\right)}\middle|\begin{matrix}0\\0,0\end{matrix}\right) - G_{1,2}^{2,1}\left(\frac{\psi}{\rho a_1}\middle|\begin{matrix}0\\0,0\end{matrix}\right)\right], \tag{31c}$$

in which $\nu = \frac{1}{M\beta^2 d_{h_0}^{-\alpha} d_{h_2}^{-\alpha}}$ and $\psi = \frac{1}{d_{g_2}^{-\alpha}} + \frac{1}{\beta^2 d_{h_0}^{-\alpha} d_{h_2}^{-\alpha}}\left(\frac{1}{M} - \frac{\beta^2 d_{h_0}^{-\alpha} d_{h_2}^{-\alpha}}{d_{g_2}^{-\alpha}}\right)$ and $G_{p,q}^{m,n}[\cdot]$ is the Meijer G-function [34, Eq. (9.301)].

Proof 2: See Appendix B

Next, we have ergodic capacity at D_1 for NOMA is calculated as

$$\mathcal{C}_1 \triangleq E\left\{\frac{1}{2}\log_2\left(1+\bar{\gamma}_1\right)\right\}. \tag{32}$$

Proposition 3: The closed-form expression of ergodic capacity at user D_1 can be given by

$$\mathcal{C}_1 = \frac{1}{2\ln 2}\left[\bar{\mathcal{B}}_1 + \frac{d_{g_1}^{-\alpha}}{\left(d_{g_1}^{-\alpha} - M\beta^2 d_{h_0}^{-\alpha} d_{h_1}^{-\alpha}\right)}\left(\bar{\mathcal{B}}_2 - \bar{\mathcal{B}}_3\right)\right], \tag{33}$$

where

$$\bar{\mathcal{B}}_1 = e^{\frac{1}{\rho a_1 M\beta^2 d_{h_0}^{-\alpha} d_{h_1}^{-\alpha}}} E_1\left(\frac{1}{\rho a_1 M\beta^2 d_{h_0}^{-\alpha} d_{h_1}^{-\alpha}}\right), \tag{34a}$$

$$\bar{\mathcal{B}}_2 = e^{\frac{1}{\rho a_1 d_{g_1}^{-\alpha}}} E_1\left(\frac{1}{\rho a_1 d_{g_1}^{-\alpha}}\right), \tag{34b}$$

$$\bar{\mathcal{B}}_3 = e^{\Theta} E_1\left(\Theta\right), \tag{34c}$$

in with $\Theta = \frac{1}{\rho a_1 d_{g_1}^{-\alpha}} + \frac{1}{\rho a_1 \beta^2 d_{h_0}^{-\alpha} d_{h_1}^{-\alpha}}\left(\frac{1}{M} - \frac{\beta^2 d_{h_0}^{-\alpha} d_{h_1}^{-\alpha}}{d_{g_1}^{-\alpha}}\right)$.

Proof 3: See Appendix C

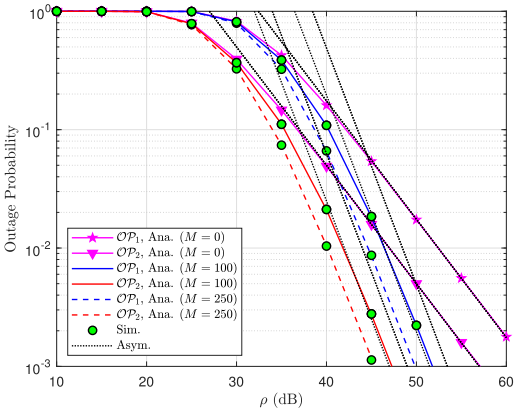

FIGURE 3. OP versus transmit SNR.

B. OMA TRANSMISSION SCHEME

In this subsection, we investigate the ergodic capacity of D for OMA

$$\begin{aligned}\mathcal{C}_D &\triangleq E\left\{\frac{1}{4}\log_2\left(1+\tilde{\gamma}_D\right)\right\}\\ &= \frac{1}{4\ln 2}\int_0^{\infty}\frac{1}{1+x}\left[1-F_{\tilde{\gamma}_D}\left(x\right)\right]dx\\ &= \frac{1}{4\ln 2}\int_0^{\infty}\frac{1}{1+x}\left[e^{-\frac{x}{M\ell_d\rho}} + \frac{d_{g_D}^{-\alpha}}{\left(d_{g_D}^{-\alpha} - M\ell_d\right)}\right.\\ &\quad\left.\times\, e^{-\frac{x}{d_{g_D}^{-\alpha}\rho}}\left(1 - e^{-\frac{x}{\ell_d\rho}\left(\frac{1}{M}-\frac{\ell_d}{d_{g_D}^{-\alpha}}\right)}\right)\right]dx.\end{aligned} \tag{35}$$

Similarly with solving of $\mathcal{C}_1$ it can be achieved $\mathcal{C}_D$ as

$$\mathcal{C}_D = \frac{1}{4\ln 2}\left[e^{\frac{1}{M\ell_d\rho}}E_1\left(\frac{1}{M\ell_d\rho}\right) + \frac{d_{g_D}^{-\alpha}}{\left(d_{g_D}^{-\alpha} - M\ell_d\right)}\right.$$
$$\left.\times\, e^{\frac{1}{d_{g_D}^{-\alpha}\rho}}E_1\left(\frac{1}{d_{g_D}^{-\alpha}\rho}\right) - e^{\Upsilon}E_1\left(\Upsilon\right)\right], \tag{36}$$

where $\Upsilon = \frac{1}{d_{g_D}^{-\alpha}\rho} + \frac{1}{\ell_d\rho}\left(\frac{1}{M} - \frac{\ell_d}{d_{g_D}^{-\alpha}}\right)$.

V. NUMERICAL RESULTS

In simulation, we set $a_1 = 0.1$ and $a_2 = 0.9$. The target rates of D_1, D_2, D are $R_1 = 1.5$, $R_2 = 1$ and $R_0 = 2$ regardless of specific cases indicated later. All simulations are statistically averaged over 10^7 independent iterations. The remaining parameters can be summarized in Table 2.

Fig. 3 plots the OP versus the SNR associated with transmission at the transmit SNR at the BS ρ. These curves precisely match the analytic values, indicating that OP indeed decreased in the high SNR region. Thus, improving SINR of signal detection can be achieved at the high SNR of the BS region. This is guideline to improve OP. Note that OP under RIS Scheme was superior to that under the context of NOMA without RIS. We can see OP of D_2 outperforms that D_1 and such OP also depends on value of M. The main reason is that

TABLE 2. Table of parameters for numerical results.

The RIS attenuation coefficient	$\beta = 0.4$
The normalised distance between the BS and the RIS	$d_{h_0} = 10$ (m)
The normalised distance between the BS and D_1	$d_{h_1} = 8$ (m)
The normalised distance between the BS and D_2	$d_{h_2} = 20$ (m)
The normalised distance between the BS and D	$d_{h_D} = 8$ (m)
The normalised distance between the RIS and D_1	$d_{g_1} = 5$ (m)
The normalised distance between the RIS and D_2	$d_{g_1} = 10$ (m)
The normalised distance between the RIS and D	$d_{g_D} = 5$ (m)
The path loss exponent	$\alpha = 2$

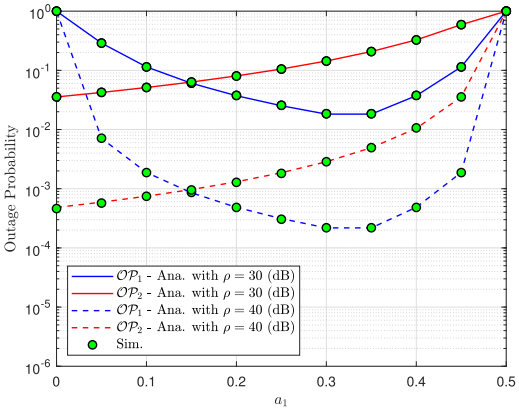

FIGURE 4. OP versus power allocation factor a_1, with $\rho = 30, 40$ (dB).

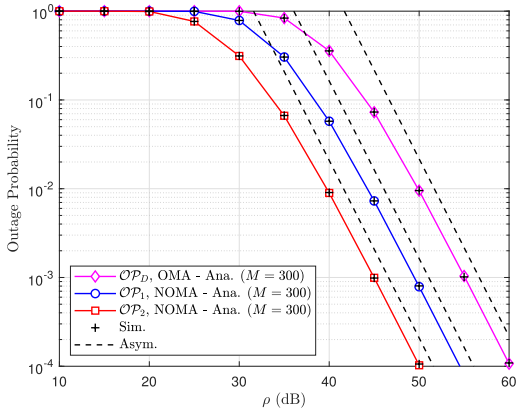

FIGURE 5. Comparison OPs between RIS-NOMA and RIS-OMA.

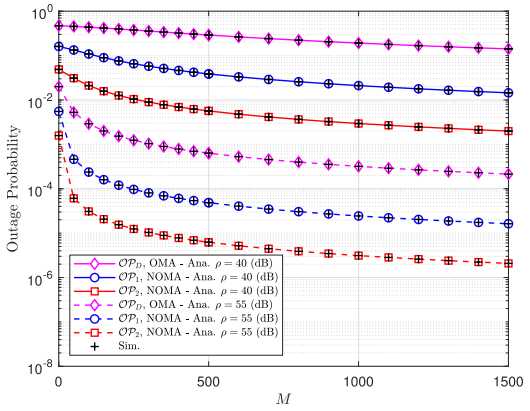

FIGURE 6. OP versus the number of reflecting elements in the RIS M.

SINRs corresponding two users depend on power allocation factor a_1, a_2 as observation in (4), (5) and (6), then condition $a_2 > a_1$ leads to such performance gap among two users. It is further conclude that more reflecting elements $M = 250$ is reported as the best performance.

Fig. 4 illustrates the optimal OP of users D_1, D_2 at several points of a_1. These results can be explained by the fact that power allocation factors a_1 and a_2 contribute to the variation in SINR as well as the corresponding OP, especially it exhibits optimal OP for D_1 at $a_1 = 0.35$. These result also demonstrate that varying the number of RIS cells has only a negligible influence on OP, as indicated by the two cases of M within the observed region. It is intuitively seen that high transmit SNR at the BS result in better outage performance.

Fig. 5 depicts the role of NOMA in increasing spectrum efficiency for RIS-aided wireless system. In particular, the RIS using NOMA outperforms than that using OMA. It can explained that RIS using OMA needs higher time slots to send signal s_1, s_2, which reduce system performance. Other trends of OP curves can be seen similarly as previous figures.

Fig. 6 illustrates the improvement of OP for RIS-NOMA and RIS-OMA at very high number of reflecting elements, $M = 1500$. From this figure, it becomes evident that the analytical results indicate that OP can be improved at high value of M; thus, verifying the important role of RIS in design of the presented theoretical framework. However, the cost of RIS needs be studied to achieve OP improvement. Additionally, it is observed that, as M increases for many situations, the equivalent OP also increases, but at high M, the OP is limited by the target rates, and thus such OP can not improve more. This indicates that by selecting suitable value of M, we can improve the diversity gain of the RIS-assisted wireless system.

Fig. 7 confirmed that the throughput meets the ceiling as target rates at high region of SNR, ρ. It can be seen throughput of user D_2 can approach maximum value sooner than other cases due to its outage performance is evaluated as best case in previous figures. Such observations are consistent with the expressions calculated in (24a) and (24b).

We can see similar outage behavior for case of without direct link as Fig. 8. In particular, although smaller M is required, we can achieve reasonable outage performance, i.e. $M = 30$ is reported as best case. Since (19), (21) contain target rate, and such rates limit performance of the OP metric. We can see such trend as Fig. 9, where the OP performance is too bad when target rates reach to 1.8. Further, by comparing OP performance of the RIS-NOMA system with and without direct link, we conclude that it is acceptable to implement the

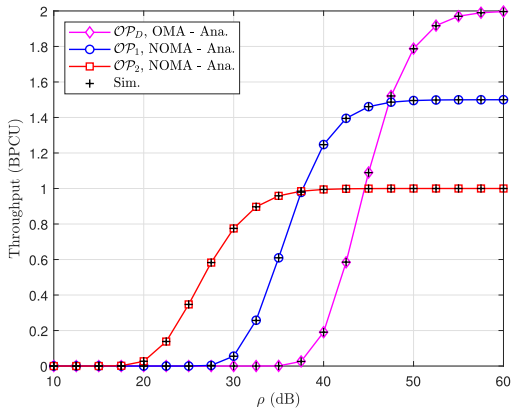

FIGURE 7. Throughput versus transmit SNR at the BS, with $M = 300$.

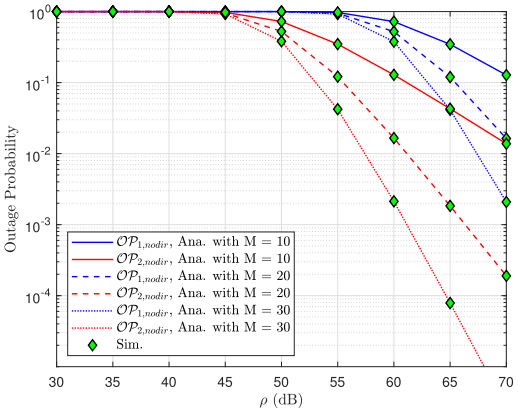

FIGURE 8. The OP versus transmit SNR at the BS for RIS-NOMA without direct link.

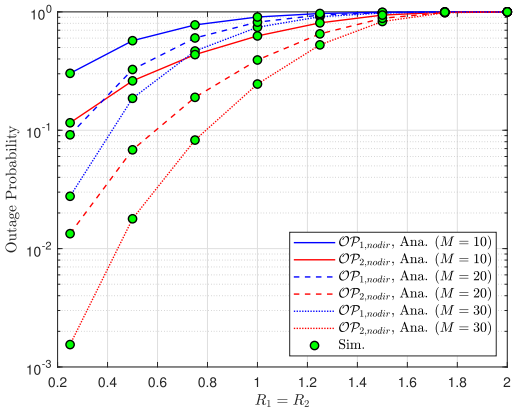

FIGURE 9. The OP versus the target rates for the RIS-NOMA without direct link, $a_1 = 0.05$, $a_2 = 0.95$ and $\rho = 50$ (dB).

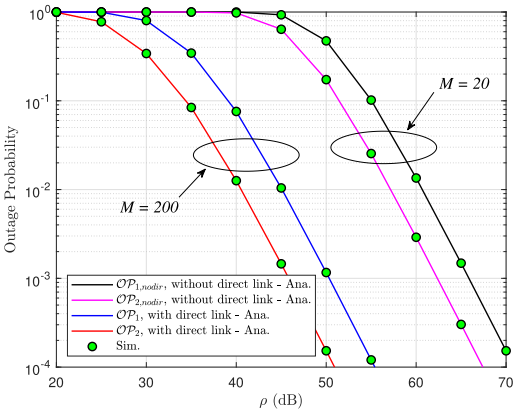

FIGURE 10. The OP comparison between the RIS-NOMA with and without direct link.

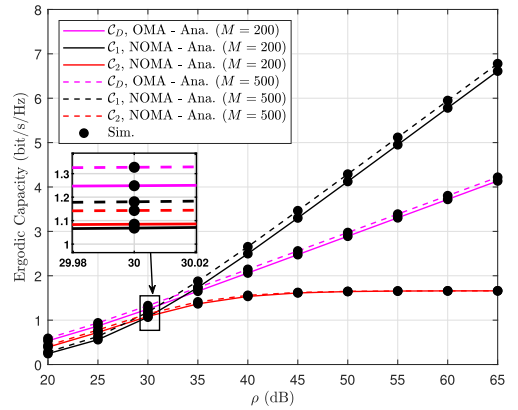

FIGURE 11. Ergodic capacity versus transmit SNR at the BS.

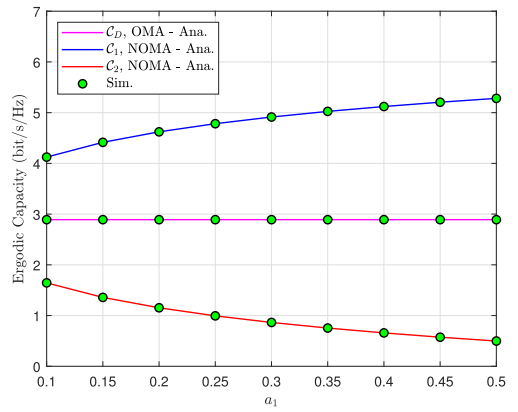

FIGURE 12. The impact of a_1 on ergodic capacity, with $\rho = 50$(dB).

considered system since the tradeoff between the cost of RIS and OP performance is clearly seen in Fig. 10.

Fig. 11 depicts the ergodic capacity as a function of SNR ρ, for two cases of M. In more detail, the curves of ergodic capacity for user D_2 meets saturation at the high SNR, while the ergodic capacity increases significantly at high SNR for user D_1 and user using OMA transmission scheme. Further, such ergodic capacity depends on ρ rather than the number of reflecting elements in the RIS. As can be seen from figure, changing M from 200 to 500 does not improve ergodic capacity of user D_2. In contrast, slight different ergodic capacity performances can be reported at user D_1 and user using OMA. Further observation is that ipSIC case of user D_1 shows its degraded performance.

From Fig. 12, it becomes evident that the theoretical and simulation results indicate power allocation coefficient a_1 contribute significantly to two performance metrics such as OP and ergodic capacity. The reason for different trends of ergodic capacity for two users is explained by SINRs rely mostly on such power coefficient; hence, the fairness of two users should be reasonable decided. Similarly, ipSIC case of user D_1 is reported as degraded performance.

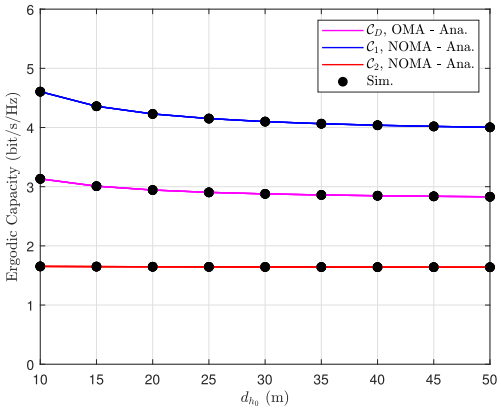

FIGURE 13. The impact of distances on ergodic performance, with $M = 1500$.

From Fig. 13, if the RIS is located far from the BS, the ergodic performance will be reduced, but such situation is not crucial. As we can see from figure, just slight decrease of ergodic capacity of two users in NOMA and user in OMA mode can be reported in this experiment. This is evident that the design of RIS in wireless system based on mostly architecture of RIS and the BS rather than locations of nodes in systems.

VI. CONCLUSION

In this study, we have adopted NOMA and OMA transmissions to illustrate how these schemes work in RIS-aided wireless systems, where the main parameters of the RIS were designed. We design two links (direct and backscatter links) to provide outage probability, ergodic capacity and throughput. It is concluded that system performance can be improved at high-SNR region and higher number of reflecting elements in the RIS. Further, RIS-NOMA outperforms than RIS-OMA in term of outage probability while ergodic capacity of the near user is reported as the best case. These expressions are also derived accompanied by simulated analysis to confirm advantages of RIS in the considered systems. In the future, we extend the proposed model to RIS-aided NOMA networks with multiple RISs and multiple antennas.

APPENDIX A
PROOF OF PROPOSITION 1

From (26), one can observe $\mathcal{OP}_{1,nodir} = 1$ when $a_2 < a_1\varepsilon_1$. As a result, $\mathcal{OP}_{1,nodir}$ can be expressed as

$$\mathcal{OP}_{1,nodir} = \left[\underbrace{\Pr\left(\left|\mathbf{v}_p^H\mathbf{D}_1\mathbf{h}_0\right|^2 < \varpi_{\max}\right)}_{\mathcal{E}}\right]^P \tag{37}$$

Based on (25), we have $\mathcal{E}$ is calculated as

$$\begin{aligned}\mathcal{E} &= \int_0^{\varpi_{\max}} f_{\left|\mathbf{v}_p^H\mathbf{D}_1\mathbf{h}_0\right|^2}(x)dx \\ &= \frac{2}{\Gamma\left(\frac{M}{P}\right)}\int_0^{\varpi_{\max}} x^{\frac{\frac{M}{P}-1}{2}} K_{\frac{M}{P}-1}\left(2\sqrt{x}\right)dx.\end{aligned} \tag{38}$$

Let $r = \sqrt{\frac{x}{\varpi_{\max}}} \rightarrow \varpi_{\max}r^2 = x \rightarrow \varpi_{\max}rdr = dx$, $\mathcal{E}$ can be reformulated by

$$\mathcal{E} = \frac{4(\varpi_{\max})^{\frac{\frac{M}{P}+1}{2}}}{\Gamma\left(\frac{M}{P}\right)}\int_0^1 r^{\frac{M}{P}} K_{\frac{M}{P}-1}\left(2\sqrt{\varpi_{\max}}r\right)dr. \tag{39}$$

With the help of [34, Eq. (6.561.8)], (39) can be given as

$$\mathcal{E} = 1 - \frac{2(\varpi_{\max})^{\frac{M}{2P}}}{\Gamma\left(\frac{M}{P}\right)}K_{\frac{M}{P}}\left(2\sqrt{\varpi_{\max}}\right). \tag{40}$$

Substituting (40) into (37), $\mathcal{OP}_{1,nodir}$ is given by

$$\mathcal{OP}_{1,nodir} = \left[1 - \frac{2(\varpi_{\max})^{\frac{M}{2P}}}{\Gamma\left(\frac{M}{P}\right)}K_{\frac{M}{P}}\left(2\sqrt{\varpi_{\max}}\right)\right]^P. \tag{41}$$

The proof is completed.

APPENDIX B
PROOF OF PROPOSITION 2

The ergodic capacity at D_2 is calculated as

$$\begin{aligned}\mathcal{C}_2 &\triangleq E\left\{\frac{1}{2}\log_2\left(1+\tilde{\gamma}_2\right)\right\} \\ &= \frac{1}{2\ln 2}\int_0^{\infty}\frac{1}{1+x}\left[1 - F_{\tilde{\gamma}_2}(x)\right]dx.\end{aligned} \tag{42}$$

By the definition of the expectation operator and after integration-by-part, $\mathcal{C}_2$ can then be evaluated as

$$\mathcal{C}_2 = \frac{1}{2\ln 2}\int_0^{\frac{a_2}{a_1}}\frac{1}{1+x}\left[1 - F_{\left|\tilde{T}_2\right|^2}\left(\frac{x}{\rho\left(a_2 - xa_1\right)}\right)\right]dx. \tag{43}$$

By the variable changing $t = \frac{x}{\rho(a_2 - xa_1)}$ and after few steps, (43) can then be further derived as

$$\begin{aligned}\mathcal{C}_2 = \frac{1}{2\ln 2}\int_0^{\infty}&\left[\frac{1}{t + \left[\rho\left(a_2 + a_1\right)\right]^{-1}} - \frac{1}{t + \left(\rho a_1\right)^{-1}}\right] \\ &\times\left[1 - F_{\left|\tilde{T}_2\right|^2}(t)\right]dt.\end{aligned} \tag{44}$$

In (44), $F_{\left|\tilde{T}_2\right|^2}(t)$ is calculated as

$$\begin{aligned}F_{\left|\tilde{T}_2\right|^2}(t) = 1 - e^{-t\nu} - &\frac{d_{g_2}^{-\alpha}e^{-\frac{t}{d_{g_2}^{-\alpha}}}}{\left(d_{g_2}^{-\alpha} - M\beta^2 d_{h_0}^{-\alpha}d_{h_2}^{-\alpha}\right)} \\ &\times\left[1 - e^{-\frac{t}{\beta^2 d_{h_0}^{-\alpha}d_{h_2}^{-\alpha}}\left(\frac{1}{M} - \frac{\beta^2 d_{h_0}^{-\alpha}d_{h_2}^{-\alpha}}{d_{g_2}^{-\alpha}}\right)}\right]dt,\end{aligned} \tag{45}$$

where $\nu = \frac{1}{M\beta^2 d_{h_0}^{-\alpha}d_{h_2}^{-\alpha}}$

Submitting (45) into (44), $\mathcal{C}_2$ is given by

$$\begin{aligned}\mathcal{C}_2 &= \frac{1}{2\ln 2}\int_0^{\infty}\left[\frac{1}{t+\left[\rho\left(a_2+a_1\right)\right]^{-1}}-\frac{1}{t+\left(\rho a_1\right)^{-1}}\right]\\ &\times\left\{e^{-\frac{t}{M\beta^2 d_{h_0}^{-\alpha}d_{h_2}^{-\alpha}}}+\frac{d_{g_2}^{-\alpha}e^{-\frac{t}{d_{g_2}^{-\alpha}}}}{\left(d_{g_2}^{-\alpha}-M\beta^2 d_{h_0}^{-\alpha}d_{h_2}^{-\alpha}\right)}\right.\\ &\left.\times\left[1-e^{-\frac{t}{\beta^2 d_{h_0}^{-\alpha}d_{h_2}^{-\alpha}}\left(\frac{1}{M}-\frac{\beta^2 d_{h_0}^{-\alpha}d_{h_2}^{-\alpha}}{d_{g_2}^{-\alpha}}\right)}\right]\right\}dt\\ &=\frac{1}{2\ln 2}\left[\bar{\mathcal{A}}_1+\frac{d_{g_2}^{-\alpha}}{\left(d_{g_2}^{-\alpha}-M\beta^2 d_{h_0}^{-\alpha}d_{h_2}^{-\alpha}\right)}\left(\bar{\mathcal{A}}_2-\bar{\mathcal{A}}_3\right)\right],\end{aligned}\tag{46}$$

with $\bar{\mathcal{A}}_1$, $\bar{\mathcal{A}}_2$ and $\bar{\mathcal{A}}_3$ are calculated by

$$\bar{\mathcal{A}}_1=\left[G_{1,2}^{2,1}\left(\frac{\nu}{\rho\left(a_2+a_1\right)}\middle|\begin{matrix}0\\0,0\end{matrix}\right)-G_{1,2}^{2,1}\left(\frac{\nu}{\rho a_1}\middle|\begin{matrix}0\\0,0\end{matrix}\right)\right],\tag{47}$$

in which $\nu=\frac{1}{M\beta^2 d_{h_0}^{-\alpha}d_{h_2}^{-\alpha}}$, $G_{p,q}^{m,n}[\cdot]$ is the Meijer G-function [34, Eq. (9.301)]. In doing so, we make use of the equalities [35, Eq. (2.6)] as

$$\frac{1}{t+A}=\frac{1}{A}G_{1,1}^{1,1}\left(\frac{t}{A}\middle|\begin{matrix}0\\0\end{matrix}\right),\tag{48a}$$

$$e^{-\frac{t}{B}}=G_{0,1}^{1,0}\left(\frac{t}{B}\middle|\begin{matrix}-\\0\end{matrix}\right),\tag{48b}$$

respectively, and with the help of the [34, Eq. (7.811)] we can obtain (47).

Similarly, we have $\bar{\mathcal{A}}_2$ and $\bar{\mathcal{A}}_3$ are given as

$$\bar{\mathcal{A}}_2=\left[G_{1,2}^{2,1}\left(\frac{d_{g_2}^{\alpha}}{\rho\left(a_2+a_1\right)}\middle|\begin{matrix}0\\0,0\end{matrix}\right)-G_{1,2}^{2,1}\left(\frac{d_{g_2}^{\alpha}}{\rho a_1}\middle|\begin{matrix}0\\0,0\end{matrix}\right)\right],\tag{49a}$$

$$\bar{\mathcal{A}}_3=\left[G_{1,2}^{2,1}\left(\frac{\psi}{\rho\left(a_2+a_1\right)}\middle|\begin{matrix}0\\0,0\end{matrix}\right)-G_{1,2}^{2,1}\left(\frac{\psi}{\rho a_1}\middle|\begin{matrix}0\\0,0\end{matrix}\right)\right],\tag{49b}$$

where $\psi=\frac{1}{d_{g_2}^{-\alpha}}+\frac{1}{\beta^2 d_{h_0}^{-\alpha}d_{h_2}^{-\alpha}}\left(\frac{1}{M}-\frac{\beta^2 d_{h_0}^{-\alpha}d_{h_2}^{-\alpha}}{d_{g_2}^{-\alpha}}\right)$.

Combining (49b), (49a) and (47), we can obtain (30).

The proof 2 is completed.

APPENDIX C
PROOF OF PROPOSITION 3

The ergodic capacity at D_1 is calculated as

$$\begin{aligned}\mathcal{C}_1 &= E\left\{\frac{1}{2}\log_2\left(1+\bar{\gamma}_1\right)\right\}\\ &= E\left\{\frac{1}{2}\log_2\left(1+\underbrace{\rho a_1\left|\tilde{T}_1\right|^2}_{X}\right)\right\}\\ &=\frac{1}{2\ln 2}\int_0^{\infty}\frac{1}{1+x}\left[1-F_X\left(x\right)\right]dx\end{aligned}\tag{50}$$

In (12), we have $F_X(x)$ is given by

$$\begin{aligned}F_X\left(x\right) &= 1-e^{-\frac{x}{\rho a_1 M\beta^2 d_{h_0}^{-\alpha}d_{h_1}^{-\alpha}}}-\frac{d_{g_1}^{-\alpha}}{\left(d_{g_1}^{-\alpha}-M\beta^2 d_{h_0}^{-\alpha}d_{h_1}^{-\alpha}\right)}\\ &\times e^{-\frac{x}{\rho a_1 d_{g_1}^{-\alpha}}}\left[1-e^{-\frac{x}{\rho a_1\beta^2 d_{h_0}^{-\alpha}d_{h_1}^{-\alpha}}\left(\frac{1}{M}-\frac{\beta^2 d_{h_0}^{-\alpha}d_{h_1}^{-\alpha}}{d_{g_1}^{-\alpha}}\right)}\right].\end{aligned}\tag{51}$$

Substituting (51) into (50), $\mathcal{C}_1$ is calculated by

$$\begin{aligned}\mathcal{C}_1 &= \frac{1}{2\ln 2}\int_0^{\infty}\frac{1}{1+x}\left\{e^{-\frac{x}{\rho a_1 M\beta^2 d_{h_0}^{-\alpha}d_{h_1}^{-\alpha}}}\right.\\ &+\frac{d_{g_1}^{-\alpha}}{\left(d_{g_1}^{-\alpha}-M\beta^2 d_{h_0}^{-\alpha}d_{h_1}^{-\alpha}\right)}e^{-\frac{x}{\rho a_1 d_{g_1}^{-\alpha}}}\\ &\left.\times\left[1-e^{-\frac{x}{\rho a_1\beta^2 d_{h_0}^{-\alpha}d_{h_1}^{-\alpha}}\left(\frac{1}{M}-\frac{\beta^2 d_{h_0}^{-\alpha}d_{h_1}^{-\alpha}}{d_{g_1}^{-\alpha}}\right)}\right]\right\}dx\\ &=\frac{1}{2\ln 2}\left[\bar{\mathcal{B}}_1+\frac{d_{g_1}^{-\alpha}\left(\bar{\mathcal{B}}_2-\bar{\mathcal{B}}_3\right)}{\left(d_{g_1}^{-\alpha}-M\beta^2 d_{h_0}^{-\alpha}d_{h_1}^{-\alpha}\right)}\right].\end{aligned}\tag{52}$$

Then, $\bar{\mathcal{B}}_1$ is calculated as

$$\bar{\mathcal{B}}_1=\int_0^{\infty}\frac{1}{1+x}e^{-\frac{x}{\rho a_1 M\beta^2 d_{h_0}^{-\alpha}d_{h_1}^{-\alpha}}}dx.\tag{53}$$

Using [34, Eq. (3.352.4)], $\bar{\mathcal{B}}_1$ is given as

$$\begin{aligned}\bar{\mathcal{B}}_1 &= -e^{\frac{1}{\rho a_1 M\beta^2 d_{h_0}^{-\alpha}d_{h_1}^{-\alpha}}}Ei\left(-\frac{1}{\rho a_1 M\beta^2 d_{h_0}^{-\alpha}d_{h_1}^{-\alpha}}\right)\\ &= e^{\frac{1}{\rho a_1 M\beta^2 d_{h_0}^{-\alpha}d_{h_1}^{-\alpha}}}E_1\left(\frac{1}{\rho a_1 M\beta^2 d_{h_0}^{-\alpha}d_{h_1}^{-\alpha}}\right),\end{aligned}\tag{54}$$

where $Ei(-x)=-E_1(x)$ is exponential integral function.

Similarly, with solving of (54) it can be achieved $\bar{\mathcal{B}}_2$ and $\bar{\mathcal{B}}_3$ as

$$\bar{\mathcal{B}}_2=e^{\frac{1}{\rho a_1 d_{g_1}^{-\alpha}}}E_1\left(\frac{1}{\rho a_1 d_{g_1}^{-\alpha}}\right),\tag{55a}$$

$$\bar{\mathcal{B}}_3=e^{\Theta}E_1\left(\Theta\right),\tag{55b}$$

where $\Theta=\frac{1}{\rho a_1 d_{g_1}^{-\alpha}}+\frac{1}{\rho a_1\beta^2 d_{h_0}^{-\alpha}d_{h_1}^{-\alpha}}\left(\frac{1}{M}-\frac{\beta^2 d_{h_0}^{-\alpha}d_{h_1}^{-\alpha}}{d_{g_1}^{-\alpha}}\right)$

Combining (55b), (55a) and (54), we can obtain (33).

The proof 3 is completed.

REFERENCES

[1] Q.-U.-U. Nadeem, A. Kammoun, A. Chaaban, M. Debbah, and M.-S. Alouini, "Intelligent reflecting surface assisted wireless communication: Modeling and channel estimation," 2019, *arXiv:1906.02360*. [Online]. Available: http://arxiv.org/abs/1906.02360

[2] Y.-C. Liang, R. Long, Q. Zhang, J. Chen, H. V. Cheng, and H. Guo, "Large intelligent surface/antennas (LISA): Making reflective radios smart," *J. Commun. Inf. Netw.*, vol. 4, no. 2, pp. 40–50, Jun. 2019.
[3] L. Yang, F. Meng, Q. Wu, D. B. da Costa, and M.-S. Alouini, "Accurate closed-form approximations to channel distributions of RIS-aided wireless systems," *IEEE Wireless Commun. Lett.*, vol. 9, no. 11, pp. 1985–1989, Nov. 2020.
[4] D. Mishra and H. Johansson, "Channel estimation and low-complexity beamforming design for passive intelligent surface assisted MISO wireless energy transfer," in *Proc. IEEE Int. Conf. Acoust., Speech Signal Process. (ICASSP)*, May 2019, pp. 4659–4663.
[5] C. Huang, A. Zappone, G. C. Alexandropoulos, M. Debbah, and C. Yuen, "Reconfigurable intelligent surfaces for energy efficiency in wireless communication," *IEEE Trans. Wireless Commun.*, vol. 18, no. 8, pp. 4157–4170, Aug. 2019.
[6] Q. Wu and R. Zhang, "Towards smart and reconfigurable environment: Intelligent reflecting surface aided wireless network," *IEEE Commun. Mag.*, vol. 58, no. 1, pp. 106–112, Jan. 2020.
[7] Q. Wu and R. Zhang, "Intelligent reflecting surface enhanced wireless network: Joint active and passive beamforming design," in *Proc. IEEE Global Commun. Conf. (GLOBECOM)*, Dec. 2018, pp. 1–6.
[8] Q. Nadeem, A. Kammoun, A. Chaaban, M. Debbah, and M.-S. Alouini, "Large intelligent surface assisted MIMO communications," 2019, *arXiv:1903.08127*. [Online]. Available: https://arxiv.org/abs/1903.08127
[9] H. Zhang, B. Di, L. Song, and Z. Han, "Reconfigurable intelligent surfaces assisted communications with limited phase shifts: How many phase shifts are enough?" *IEEE Trans. Veh. Technol.*, vol. 69, no. 4, pp. 4498–4502, Apr. 2020.
[10] E. Basar, "Reconfigurable intelligent surface-based index modulation: A new beyond MIMO paradigm for 6G," *IEEE Trans. Commun.*, vol. 68, no. 5, pp. 3187–3196, May 2020.
[11] A. Ranjha and G. Kaddoum, "URLLC facilitated by mobile UAV relay and RIS: A joint design of passive beamforming, blocklength and UAV positioning," *IEEE Internet Things J.*, early access, Sep. 28, 2020, doi: 10.1109/JIOT.2020.3027149.
[12] S. Lin, B. Zheng, G. C. Alexandropoulos, M. Wen, M. Di Renzo, and F. Chen, "Reconfigurable intelligent surfaces with reflection pattern modulation: Beamforming design and performance analysis," *IEEE Trans. Wireless Commun.*, vol. 20, no. 2, pp. 741–754, Feb. 2021, doi: 10.1109/TWC.2020.3028198.
[13] C. Huang, A. Zappone, M. Debbah, and C. Yuen, "Achievable rate maximization by passive intelligent mirrors," in *Proc. IEEE Int. Conf. Acoust., Speech Signal Process. (ICASSP)*, Calgary, AB, Canada, Apr. 2018, pp. 3714–3718.
[14] C. Huang, G. C. Alexandropoulos, A. Zappone, M. Debbah, and C. Yuen, "Energy efficient multi-user MISO communication using low resolution large intelligent surfaces," in *Proc. IEEE Globecom Workshops (GC Wkshps)*, Abu Dhabi, UAE, Dec. 2018, pp. 1–6.
[15] G. Lee, M. Jung, A. T. Z. Kasgari, W. Saad, and M. Bennis, "Deep reinforcement learning for energy-efficient networking with reconfigurable intelligent surfaces," in *Proc. IEEE Int. Conf. Commun. (ICC)*, Dublin, Ireland, Jun. 2020, pp. 1–6.
[16] S. Atapattu, R. Fan, P. Dharmawansa, G. Wang, and J. Evans, "Two–way communications via reconfigurable intelligent surface," in *Proc. IEEE Wireless Commun. Netw. Conf. (WCNC)*, Seoul, South Korea, May 2020, pp. 1–6.
[17] A. Taha, M. Alrabeiah, and A. Alkhateeb, "Enabling large intelligent surfaces with compressive sensing and deep learning," Apr. 2019, *arXiv:1904.10136*. [Online]. Available: http://arxiv.org/abs/1904.10136
[18] X. Yu, D. Xu, and R. Schober, "Enabling secure wireless communications via intelligent reflecting surfaces," 2019, *arXiv:1904.09573*. [Online]. Available: http://arxiv.org/abs/1904.09573
[19] E. Basar, "Transmission through large intelligent surfaces: A new frontier in wireless communications," in *Proc. Eur. Conf. Netw. Commun. (EuCNC)*, Valencia, Spain, Jun. 2019, pp. 112–117.
[20] L. Du, C. Huang, W. Guo, J. Ma, X. Ma, and Y. Tang, "Reconfigurable intelligent surfaces assisted secure multicast communications," *IEEE Wireless Commun. Lett.*, vol. 9, no. 10, pp. 1673–1676, Oct. 2020.
[21] X. Li, M. Zhao, Y. Liu, L. Li, Z. Ding, and A. Nallanathan, "Secrecy analysis of ambient backscatter NOMA systems under I/Q imbalance," *IEEE Trans. Veh. Technol.*, vol. 69, no. 10, pp. 12286–12290, Oct. 2020, doi: 10.1109/TVT.2020.3006478.
[22] T.-L. Nguyen and D.-T. Do, "Power allocation schemes for wireless powered NOMA systems with imperfect CSI: An application in multiple antenna-based relay," *Int. J. Commun. Syst.*, vol. 31, no. 15, p. e3789, Oct. 2018.
[23] X. Li, Q. Wang, Y. Liu, T. A. Tsiftsis, Z. Ding, and A. Nallanathan, "UAV-aided multi-way NOMA networks with residual hardware impairments," *IEEE Wireless Commun. Lett.*, vol. 9, no. 9, pp. 1538–1542, Sep. 2020.
[24] D.-T. Do, M.-S.-V. Nguyen, F. Jameel, R. Jantti, and I. S. Ansari, "Performance evaluation of relay-aided CR-NOMA for beyond 5G communications," *IEEE Access*, vol. 8, pp. 134838–134855, 2020.
[25] D.-T. Do, T.-L. Nguyen, K. M. Rabie, X. Li, and B. M. Lee, "Throughput analysis of multipair two-way replaying networks with NOMA and imperfect CSI," *IEEE Access*, vol. 8, pp. 128942–128953, 2020.
[26] D.-T. Do, A.-T. Le, and B. M. Lee, "NOMA in cooperative underlay cognitive radio networks under imperfect SIC," *IEEE Access*, vol. 8, pp. 86180–86195, 2020.
[27] D.-T. Do and A.-T. Le, "NOMA based cognitive relaying: Transceiver hardware impairments, relay selection policies and outage performance comparison," *Comput. Commun.*, vol. 146, pp. 144–154, Oct. 2019.
[28] T. Hou, Y. Liu, Z. Song, X. Sun, Y. Chen, and L. Hanzo, "Reconfigurable intelligent surface aided NOMA networks," *IEEE J. Sel. Areas Commun.*, vol. 38, no. 11, pp. 2575–2588, Nov. 2020.
[29] X. Liu, Y. Liu, Y. Chen, and H. V. Poor, "RIS enhanced massive non-orthogonal multiple access networks: Deployment and passive beamforming design," *IEEE J. Sel. Areas Commun.*, early access, Aug. 24, 2020, doi: 10.1109/JSAC.2020.3018823.
[30] T. Hou, Y. Liu, Z. Song, X. Sun, and Y. Chen, "MIMO-NOMA networks relying on reconfigurable intelligent surface: A signal cancellation-based design," *IEEE Trans. Commun.*, vol. 68, no. 11, pp. 6932–6944, Nov. 2020, doi: 10.1109/TCOMM.2020.3018179.
[31] Z. Yang, J. Shi, Z. Li, M. Chen, W. Xu, and M. Shikh-Bahaei, "Energy efficient rate splitting multiple access (RSMA) with reconfigurable intelligent surface," in *Proc. IEEE Int. Conf. Commun. Workshops (ICC Workshops)*, Dublin, Ireland, Jun. 2020, pp. 1–6.
[32] W. Zhao, G. Wang, S. Atapattu, T. A. Tsiftsis, and C. Tellambura, "Is backscatter link stronger than direct link in reconfigurable intelligent surface-assisted system?" *IEEE Commun. Lett.*, vol. 24, no. 6, pp. 1342–1346, Jun. 2020.
[33] Z. Ding, R. Schober, and H. V. Poor, "On the impact of phase shifting designs on IRS-NOMA," *IEEE Wireless Commun. Lett.*, vol. 9, no. 10, pp. 1596–1600, Oct. 2020.
[34] I. S. Gradshteyn and I. M. Ryzhik, *Tables of Integrals, Series and Products*, 6th ed. New York, NY, USA: Academic, 2000.
[35] A. Mathai, R. Saxena, and H. Haubold, *The H-Function: Theory and Applications*. New York, NY, USA: Springer, 2009.
[36] Z. Ding and H. V. Poor, "A simple design of IRS-NOMA transmission," *IEEE Commun. Lett.*, vol. 24, no. 5, pp. 1119–1123, May 2020.
[37] X. Yue and Y. Liu, "Performance analysis of intelligent reflecting surface assisted NOMA networks," Feb. 2020, *arXiv:2002.09907*. [Online]. Available: https://arxiv.org/abs/2001.09907

CHI-BAO LE was born in Binh Thuan, Vietnam. He is currently pursuing the master's degree in wireless communications. He has worked closely with Dr. Thuan at the Wireless Communications and Signal Processing Research Group, Industrial University of Ho Chi Minh City, Vietnam. His research interests include electronic design, signal processing in wireless communications networks, non-orthogonal multiple access, and physical layer security.

DINH-THUAN DO (Senior Member, IEEE) received the B.S., M.Eng., and Ph.D. degrees in communications engineering from Vietnam National University (VNU-HCM), in 2003, 2007, and 2013, respectively. Prior to joining Asia University, he was a Senior Engineer with the VinaPhone Mobile Network, from 2003 to 2009. He published over 85 SCI/SCIE journal articles, one sole author book, and five book chapters. His research interests include signal processing in wireless communications networks, cooperative communications, non-orthogonal multiple access, full-duplex transmission, and energy harvesting. He was a recipient of the Golden Globe Award from the Vietnam Ministry of Science and Technology, in 2015 (Top ten excellent young scientists nationwide). He has served as a guest editor for four prominent SICE journals. He is currently serving as an associate editor for six journals, including *EURASIP Journal on Wireless Communications and Networking*, *Computer Communications* (Elsevier), and *KSII Transactions on Internet and Information Systems*.

XINGWANG LI (Senior Member, IEEE) received the B.Sc. degree from Henan Polytechnic University, Jiaozuo, China, in 2007, the M.Sc. degree from the University of Electronic Science and Technology of China, in 2010, and the Ph.D. degree from the Beijing University of Posts and Telecommunications, in 2015. From 2010 to 2012, he was working with Comba Telecom Ltd., Guangzhou, China, as an Engineer. He was a Visiting Scholar with the State Key Laboratory of Networking and Switching Technology, Beijing University of Posts and Telecommunications, from 2016 to 2018. From 2017 to 2018, he was also a Visiting Scholar with Queen's University Belfast, Belfast, U.K. He is currently an Associate Professor with the School of Physics and Electronic Information Engineering, Henan Polytechnic University. His research interests include MIMO communication, cooperative communication, hardware constrained communication, non-orthogonal multiple access, physical layer security, unmanned aerial vehicles, and the Internet of Things. He has served as a member for many TPCs, such as IEEE/CIC International Conference on Communications in China (ICCC'2019) and IEEE Global Communications Conference 2018 (GLOBECOM'18). He is also an Editor on the Editorial Board of IEEE Access, *Computer Communications*, and *KSII Transactions on Internet and Information Systems*.

YUNG-FA HUANG (Member, IEEE) received the Dipl.-Eng. degree in electrical engineering from the National Taipei University of Technology, Taipei, in 1982, the M.Eng. degree in electrical engineering from National Tsing Hua University, Hsinchu, Taiwan, in 1987, and the Ph.D. degree in electrical engineering from National Chung Cheng University, Chiayi, Taiwan, in 2002. From 1982 to 1984, he joined the Air Forces for the military service in Taiwan. From 1987 to 2002, he was an Instructor with the Chung Chou Institute of Technology, Yuanlin, Taiwan. From February 2002 to July 2004, he was with the Department of Electrical Engineering, Chung Chou Institute of Technology, as an Associate Professor. From August 2004 to July 2007, he was an Associate Professor with the Graduate Institute of Networking and Communication Engineering, Chaoyang University of Technology, Taichung, Taiwan. From August 2007 to July 2008, he was the Department Head of Computer and Communication Engineering and the Institute Chair of the Graduate Institute of Networking and Communication Engineering, Chaoyang University of Technology, where he was the Department Head of Information and Communication Engineering, from August 2008 to July 2010. Since September 2012, he has been a Professor with the Department of Information and Communication Engineering, Chaoyang University of Technology. His current research interests include multiuser detection in OFDM-CDMA cellular mobile communication systems, communication signal processing, fuzzy systems, and wireless sensor networks. He serves as the Co-Chair for the IEEE SMC Society Technical Committee on Intelligent Internet Systems.

HSING-CHUNG CHEN (Senior Member, IEEE) received the Ph.D. degree in electronic engineering from National Chung Cheng University, Taiwan, in 2007. From February 2008 to July 2019, he had been an Assistant Professor, an Associate Professor, and a Full Professor with the Department of Computer Science and Information Engineering, Asia University, Taiwan. Since May 2014, he has been a Research Consultant with the Department of Medical Research, China Medical University Hospital, China Medical University, Taiwan. Since 2018, he has also been a Distinguished Full Professor with the Department of Computer Science and Information Engineering, Asia University. His current research interests include information and communication security, cyberspace security, blockchain network security, the Internet of Things application engineering and security, mobile and wireless networks protocols, medical and bio-information signal image processing, artificial intelligence and soft computing, and applied cryptography. Since February 2017, he has also been a Permanent Council Member of the Taiwan Domain Names Association (Taiwan DNA), Taiwan. He is also a member of Taiwan Fuzzy Systems Association (TFSA), ICCIT, CCISA, and IET. He had been awarded the best paper awards by BWCCA2018, MobiSec2017, and BWCCA2016, individually. He was awarded the Best Journal Paper Award by the Association for Algorithm and Computation Theory (AACT). He had also served as the Program Committee Chair for the APNIC44, in September 2017, organized by the Asia-Pacific Network Information Centre (APNIC). He was the Editor-in-Chief of the Newsletter of TWCERT/CC, from July 2012 to June 2013. He served or is serving on several general chairs, program committee chairs, workshop chairs, and technical program committees for some international conferences. He has served as a reviewer for more than 20 international journals. He serves as a Guest Editor for many international journals, such as IEEE Transactions on Industrial Informatics, IEEE Access, *Sensors*, and *Energies*.

MIROSLAV VOZNAK (Senior Member, IEEE) received the Ph.D. degree in telecommunications from the Faculty of Electrical Engineering and Computer Science, VSB-Technical University of Ostrava, in 2002, and the Habilitation degree in 2009. He was appointed as a Full Professor in electronics and communications technologies in 2017. He is the author or coauthor of more than 100 articles in SCI/SCIE journals. His research interests include information and communication technologies, especially on quality of service and experience, networks security, wireless networks, and big data analytics. He has served as a member of editorial boards for several journals, including *Sensors*, the *Journal of Communications*, *Elektronika Ir Elektrotechnika*, and *Advances in Electrical and Electronic Engineering*.